Integrating battery banks to wind farms for frequency support provision–capacity sizing and support algorithms

A. B. Attya[1]

[1] *Department of Electronic and Electrical Engineering, University of Strathclyde, Glasgow, G1 1RD, United Kingdom*

The expected high penetration levels of wind energy in power systems require robust and practical solutions to maintain typical conventional systems performance. Wind farms (WFs) positive contribution in eliminating grid frequency deviations still a grey area, especially when they replace considerable conventional generation capacities. This paper offers a sizing algorithm to integrate storage battery banks (SBs) in WFs to provide feasible power support during frequency events. This algorithm determines the required rated power and capacity of each SB inside a WF according to several constrains, including wind speed characteristics at WF location. The size of the SB is based on a statistical study for the amounts of rejected wind power, and the events of low wind production. The offered operation algorithm controls the SB charging, discharging, and standby modes based on the acquisition of different dynamic variables, for example, WF output, load demand and storage cells' state of charge. The operation algorithm aims to mitigate frequency drops, rejected wind power and maintain the battery lifetime. Both algorithms are applied on a defined sector from a genuine conventional system merged with real WS chronological records at certain locations which are candidates to host WFs. Results reveal the positive influence of SB involvement on frequency excursions clearance, in addition, wasted wind energy is mitigated since wind turbines de-loading techniques are avoided and some rejected wind power is utilized to charge the installed SBs. Precise models are integrated through MATLAB and Simulink simulation environment.

Key words— Wind power, Battery banks, Frequency drops.

Nomenclature

WT	Wind Turbine
WF	Wind Farm
DFIG	Double Fed Induction Generator
SB	Storage bank
DOD	Depth of discharge

SOC	State of charge (max and min suffixes refer to its maximum and minimum values respectively)
MPT	Maximum power tracking operation technique
C_C	Conventional capacity in MW
CGC	Conventional generation contribution (suffices: r: required, min: minimum)
SCF^{1st}	Storage contribution factor using first method
SCF^{2nd}	Storage contribution factor using second method
WS_i	Instantaneous wind speed at the wind farm
$WS_{i\text{-avg}}$	Average wind speed at the wind farm number (*i*) location within certain duration (1 year in this paper)
WS_{rated}	Wind turbine rated wind speed
NWT_k	Number of installed WTs of the same type 'k' in the same WF
PWT_k	Rated power of WT type 'k'
m_i	Number of installed WTs' types in the same WF number (*i*).
M	Number of connected WFs
CN_i	Number of cells in storage bank 'i'
ΔPC_{total}	Total average charging power rating
ΔP_{ch}	Charging power step of one cell
Δf	Frequency deviation
C_i	Storage bank 'i' ampere hour capacity
$Load_{inst.}$	Instantaneous Load Demand
$\Delta P_{disch\ i}$	Discharge power step of storage bank 'i'
TS	Continuous storage support time
Vc_i, Ic_i	rated voltage and current of storage cell of bank 'i' respectively.

1. Introduction

Wind integration in modern power systems is presently one of the most active research fields. Several risks are currently facing conventional energy generation, namely, depleted resources, high fossil fuels prices and pollutant emissions. However, all renewable energies face many obstacles avoiding high penetration levels in conventional grids. For example, wind energy high penetration levels reduce system inertia and imply ambiguous impacts on primary reserves [1]. Therefore, research efforts are directed towards simulating and analyzing system voltage and frequency attitudes at high wind energy penetration [2, 3].

Thereupon, these research works offer practical solutions to overcome possible drawbacks caused by wind energy integration.

The next paragraphs discuss the different methods offered in literature to enhance and emphasis the role played by WFs in frequency deviations elimination. Most of these methods count on wind turbine (WT) over speeding and/or de-loading. As an illustration, running the WT at higher rotational speed than its optimum value (i.e. determined according MPT [4]), makes its rotating parts store more kinetic energy. Thus, certain ratio from this kinetic energy is extracted using different control methods by decelerating the WT to certain threshold minimum rotational speed [5, 6]. The impact of conventional generators replacement by WFs on overall system inertia was studied in [7]. It concluded that DFIGs penetration in power system does not affect its total inertia if no conventional plants are displaced. Additionally, an interesting conclusive comparison is offered in [8] between controlling WT as a conventional generator using droop theory from one side to virtual inertia principle on the other side. On the other hand, WT *de-loading* can be applied using pitch angle control so that WT output power is de-rated below its optimum value. Consequently, the difference between optimum and de-loaded outputs acts as a backup to suppress any sudden deviation between load demand and generation [9]. Nevertheless, the feasibility of such method depends on the precision and speed of pitching system controller and mechanics, as well as the accuracy of wind speed (WS) measurements. The author has provided another algorithm which integrates between most of WT support algorithms during frequency events. Initial version of this algorithm is presented in [10] where support process is managed by WS categories to avoid continuous de-loading at sufficient WSs.

Through the previous discussion, WT operation deviates from MPT operation; hence some energy is wasted to provide acceptable support to the grid at frequency drops. In addition, WFs reactions are always ambiguous according to WS conditions before, during and after the frequency event. For example, at high WSs, the system is supported for longer times and the probability of second frequency drop is lessened. Conversely, the system frequency fluctuations and the probability of suffering a second drop increase at low WSs conditions. Furthermore, WT inertia and aerodynamics have a deep influence on WT participation in system frequency recovery. Therefore, integrating energy storage methods to provide the required power support seems to be more appropriate.

Literature presented several types of energy storage methods, namely, batteries banks, hydro storage, hydrogen reservoirs and flywheels [11]. This paper implements batteries banks

storage to provide a predetermined power surge in case of frequency events. In addition, the author has already examined hydro-pumped storage as source for frequency support [12].

An optimization technique counting on cost and low resolution WS data is performed through Fuzzy logic and simple artificial neural network [13]. Predetermined threshold value for the error between WFs forecasted output and actual output is selected to govern the charging/discharging process. Likewise, an inspiring algorithm depends on the same error definition in hourly forecasted power but with higher acceptable limit (i.e. up to 50%) is presented in [14]. This research work did not concentrate so much on storage size estimation but cared more for minimizing any financial penalties that might be implied on WFs' owners if WFs output power deviated beyond certain limit according to Hungarian grid code. On the other hand, some literatures were much interested in analyzing the internal parameters performance for battery bank cells, namely, current and voltage [15, 16]. The most promising part was implementing a detailed model for NaS (Sodium Sulfur) and Li-ion batteries; hence the obtained results were highly feasible and relevant. On the same track, battery voltage was governed and total number of cells was estimated such that a maximum limit of charging/discharging power is maintained [17].

Generally, the mentioned literatures utilized battery storage as a solution only for the negative influence of WS intermittent nature on output power fluctuations. In words, dispatching WF output to fulfill the required grid operators' expectations was the main target. However, there was no solid trial to exploit installed battery banks as a backup source for energy in case of frequency excursions to provide a positive support in analogy to conventional plants reactions. Three main topics should be discussed in this field, markedly, battery bank sizing, charge/discharge control and the expected impact on system frequency. The required storage capacity estimation is related to probabilistic forecasting for WS at certain location. In addition, the capacity design aim to optimize the depth of discharge (DOD) such that battery life is intensively extended [18]. The charging and discharging durations are also considered to judge the required ampere hour capacity to allow the extraction of all stored energy at certain power level.

This paper aims two targets; estimating the required storage capacity for each WF, and controlling the SB charging-discharging procedure to provide reliable and feasible frequency support. Driving the SB through charging process during wind energy rejection (i.e. the word 'rejection' refers to the presence of excess wind energy rejected by the grid according to certain criterion as explained later) and discharging it during frequency events are innovative contributions. The offered algorithm is comprehensive as it could be applied on any WF and

any grid. As an illustration, the sizing algorithm requires chronological data for WS (or wind power production), load demand, and the generation could be assumed fully reliable, as the case in this paper or their outage data could be involved. In addition, the types and numbers of WTGs inside each WF and the basic technical specifications of the installed SBs are required. These data are available for any grid and any WF at different levels of time resolution and accuracy. On the other hand, the dual-mode operation algorithm could be applied to any SB. The requirements are instantaneous measurements for the WF production and the grid load demand. The other signals are already required for any control method (e.g. SOC and Δf). Moreover, it does not require special control on WTs and it provides a fixed predetermined power support at any frequency event.

The implied test system is a medium sized sector from a real system, namely, the Egyptian grid so that the merits, drawbacks and possible further modifications are identified.

This paper is composed of seven sections including this introduction. Next section presents the applied storage bank sizing algorithm while the third section explains SB control procedure. Fourth section summarizes essential data about the concerned hypothetical test system and the candidate locations for WFs construction. Case studies are described in section five. Results are conducted in sixth section accompanied with a comprehensive discussion, finally, Section seven concludes.

2. Assessment of storage bank rated power

Sizing of SB should compromise between economical side and technical aspects. However, this paper concentrates on technical side such that the negative impacts of high wind energy penetration levels are mitigated. Proposed algorithm acknowledges WS chronological records in WF location and the acceptable level of conventional generation participation in load coverage (i.e. generation mix) at normal operation. In other words, the amount of rejected wind energy is related to maintaining the participation ratio of conventional generation within certain boundary according to dynamic acquisition for load and WFs output variations.

The next steps describes implemented algorithm to determine the maximum possible expected charging power, thereupon the required rated power and capacity of the SB:

1. WS data at specified site are obtained in acceptable time resolution (e.g. high resolution means average WS value every 20 or 30 s) based on the actual WSs records within the considered time span (e.g. 1 day). It is of note that, the WS or WFs output forecasting is out of the scope of this paper, however, the proposed algorithm is applicable for forecasted data

or historical records of moderate resolution (the obtained SB size is altered based on the accuracy and the resolution of the available data).

2. WS arrays are incorporated with WFs' models to get WFs' output power arrays. In this paper, WS is assumed to be typical through the whole WF. Thus, the aggregation of installed WTs equals the output of any WT multiplied by the number of WTs inside the WF.

3. Required conventional generation contribution in load feed (CGC_r) is selected which is a percentage from total conventional capacity (C_c). For example, when CGC_r = 70%, conventional generation output *fluctuates* around this value during normal operation, according to the received control signals regarding load and WFs output discrepancies. Generally, the CGC_{min} is decided by system operators (in this paper, WFs output participation in load feeding should not exceed 50%). As an illustration, instantaneous wind power penetration in generation mix should not increase above certain levels to maintain system inertia and reserve [1]. When WFs outputs are high so that CGC_{min} is violated, excess wind energy is rejected by the system. The power rejection takes place through the reduction of WTGs output by violating the MPT conditions; however, this is not from the paper interests. In the simulation model a limiter is integrated to insure that the WF instantaneous output is not violating maximum allowed penetration ratio with respect to the demand. It is of note that, conventional contribution in load feed is controlled based on load demand variations. And according to the adjusted thresholds (i.e., CGC_r and CGC_{min}), the process of wind power storage and rejection is supervised.

4. Expected chronological load data should be available within the examined time span. Afterwards, the events at which the load is greater than desired conventional generation contribution (i.e. GCG_r*C_c) are gathered in "Array1" using Eq(1). Note that, Array 1 keeps the time instant at which each event occurred. Thereupon, each instant in resultant array from the previous step is subtracted from the corresponding output power of all integrated WFs at the same instant using Eq(2). Hence, the *positive events in Array 2 refer to WFs rejected power* which could be imposed to charge battery banks. Thus, SB energy capacity and rated power could be estimated. It is worth mentioning that, low CGC_r leads to remarkable reduction in the density of rejection events as shown later.

Array 1 = Negative values of (Load-$C_C \cdot CGC_r$) Eq(1)

Array 2 = Positive values of (WFs output – |Array1|) Eq(2)

5. The average of rejected power events obtained in Step 4 is calculated to get an initial value for SBs power rating based on the average charging power rating (ΔPC_{total}). Nevertheless, it is unrealistic to design storage stations to handle all the expected rejected energy for

economic reasons. Most probably this rejected energy will not be fully utilized (i.e., when it is stored) as demonstrated by mentioned literatures. Therefore, the expected rejected power should be reduced by a roughly assumed ratio, namely, 20% as in this paper. This percentage is inspired by some outcomes of previous literature. However, this reduction ratio could be accurately evaluated using probability studies (e.g. Monte Carlo Simulation).

A distributed hybrid system (SB for each WF) is implemented instead of one large centralized SB. This returns to the higher reliability of this pattern and the reduced losses, where each SB is charged directly from the adjacent WF (i.e. losses due to charging power transmission is almost avoided). In addition, the charging of SB is only dependent on its SOC and the WF generation. Moreover, during frequency events in real system, when the supporting active power is injected from diversely allocated plants the frequency recovery is smoothed. The precise location of the SB inside the WF doesn't have a major impact on its role of supporting system during frequency drops. However, it is preferred to construct SB hangar near the substation which connects the WF to the grid (point of common coupling).

The rated power of each SB is estimated through a fixed ratio called Storage Contribution Factor (SCF_i). The parameter SCF is an innovation for this paper. It is a simple parameter to distribute the overall required storage capacity between the connected WFs. Thereupon; SCF_i is multiplied by ΔPC_{total} to get the required rated power of the installed SB at each WF. Two procedures are suggested to evaluate SCF:

In the *first method*, SCF_i^{1st} is evaluated using Eq(3).

$$SCF_i^{1^{st}} = \frac{\frac{WS_{i-avg}}{m_i} * \sum_{k=1}^{k=m} \frac{PWT_k * NWT_k}{WS_{rated\ k}}}{\sum_{i=1}^{M} (\frac{WS_{i-avg}}{m_i} * \sum_{k=1}^{k=m} \frac{PWT_k * NWT_k}{WS_{rated\ k}})} \qquad \text{Eq(3)}$$

This formula is evaluated according to the participation of each 'WT_k' type (i.e. ratio between the number and rating of each WT type with respect to other types installed in the same WF). Then a resultant value is obtained for all WTs types taking into consideration the annual average WS at the WF location. This simplified method is applied to minimize further simulation and computational efforts (compared to second method as shown next).

Second method counts on WFs output power arrays obtained in the second step of the main algorithm. Particularly, at each time step the WF_i output power is divided on the overall WFs output. Afterwards, an average value for all ratios within the considered time span is calculated (SCF^{2nd}_i). However, this algorithm requires enormous simulation and computational efforts when it is applied on the whole year chronological data. In this paper, it

is applied only on four specific days, markedly, the days of highest average loads in each weather season as shown in Table (1).

Finally, a compromise between the two methods is applied using Eq(4). This compromise is applicable since the considered time span (i.e. 4 days) is relatively short, so that both methods are computationally feasible. Moreover, integrating the two methods reduces possible higher error in the first one. However, literature has also calculated storage power ratings using other simplified methods. For example, the storage power rating is a fixed percentage from WF overall capacity, namely, 10-15% according to the results obtained in [16, 17].

$$SCF_i = \frac{SCF_i^{1st} + SCF_i^{2nd}}{\sum_{i=1}^{M}\left(SCF_i^{1st} + SCF_i^{2nd}\right)} \qquad \text{Eq(4)}$$

The number of battery cells required for each WF SB is estimated based on the power rating of the selected cell type. Consequently, the number of cells (CN_i) composing each SB is obtained. An illustrative flowchart for the prosed sizing algorithm is displayed in Figure 1.

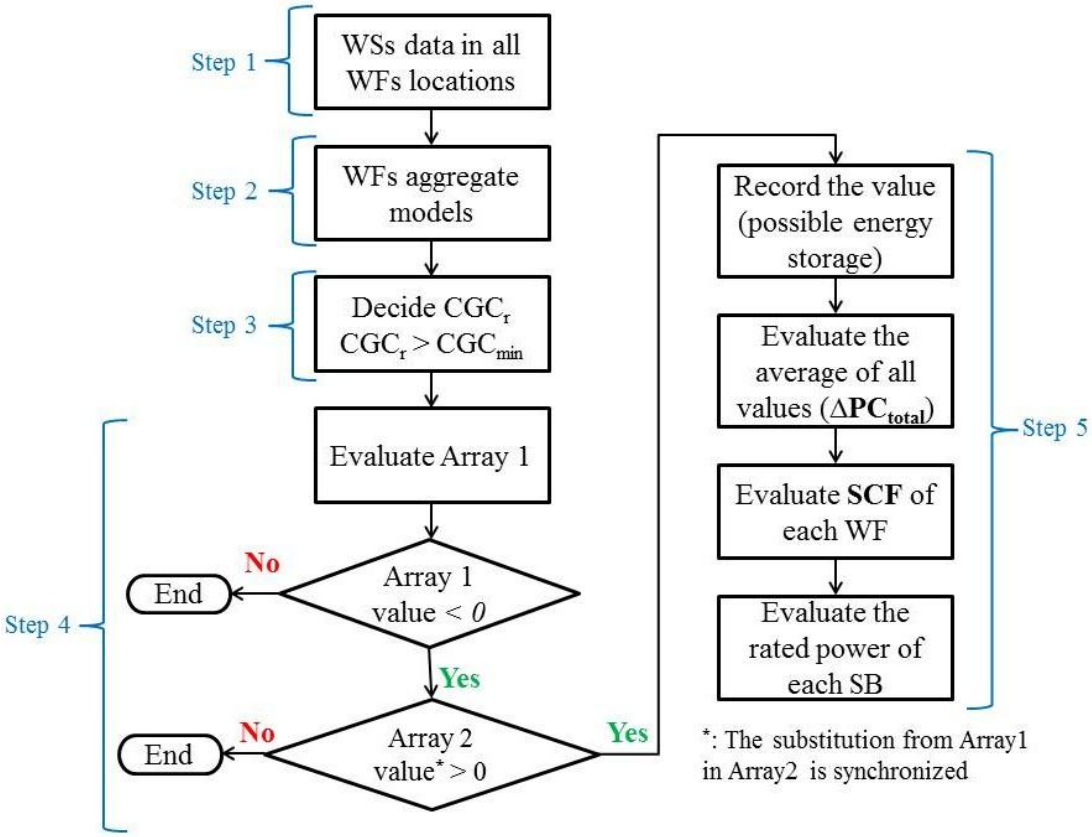

Figure 1 Sizing algorithm flowchart

Table 1 Four sample days according to Egyptian load data

Season	Winter	Spring	Summer	Fall
24Hrs average load, GW	14.9	13.2	14.6	16.3
From-to (hours in year)	217-240	4273-4296	6529-6552	7561-7584

3. Battery bank operation

Proposed algorithm splits into Normal and Support operation and it depends on four control signals, markedly, load demand, WFs output power, SOC and frequency deviation (Δf).

3.1 Normal Operation

Two possibilities are considered in this operation region, namely, charging and standby (i.e. neither charging nor discharging) modes. Charging activation requires the overlap of the following conditions:

- $SOC_{min} \leq SOC < SOC_{max}$
- $[(Load_{inst.} - CGC_r \cdot C_C) \cdot SCF_i] > WF_i$ output (i.e. the presence of excess power in WF_i)

SCF_i has a different application in second condition since it represents the expected share of WFi in load coverage. The monitoring of the second condition requires a compact data acquisition system which receives instantaneous load ($Load_{inst.}$) and WF_i output in a reasonable time step. The selection of SOC_{max} and SOC_{min} is related to DOD which has a severe impact on battery lifetime [13]. The SB is charged with a power step (ΔP_{ch}) obtained using Eq(5). ΔP_{ch} is handled by certain number of AC/DC converters as shown in Figure 2. It is of note that during charging the SB the WF continues feeding the grid with certain amount of power decided by (5), where it is the negative component of the left hand side.

$$\Delta P_{ch\,i} = WF_i\ output - (Load_{inst.} - CGC \cdot C_C) \cdot SCF_i / CN_i \qquad \text{Eq(5)}$$

Nevertheless, the share of each storage cell from ΔP_{ch} should not violate the rated current and voltage of the installed cell type. Particularly, when the output of WF is high so that ΔP_{ch} violates SB ratings; the extra power is directed to feed the existing load; hence, CGC_r is decreased below its predetermined value. Thus, conventional generators output is reduced, in parallel with suitable adjustments in the converters which control the power flow from WF to grid and SB. Hence, the amounts of wasted or rejected wind power are reduced. The number of integrated converters counts on the ratings and available budget for power electronics devices. Some literature preferred a single converter for each group of cells; in other approaches; one converter (i.e. DC/AC) ties between the SB and the power system. For simulation simplicity, the ΔP_{ch} is interpreted into a charging DC current fed into the storage cell model using Eq(6), where V_{ci} and I_{ci} are the rated voltage and current of SB cell respectively. It is worth mentioning that, the minor losses and time delays of power electronics devices are ignored.

$$i_{\text{charging}} = \frac{\Delta P_{\text{ch}}}{V_{ci} \cdot CN_i}; \quad i_{\text{charging}} \le I_{ci} \qquad \text{Eq(6)}$$

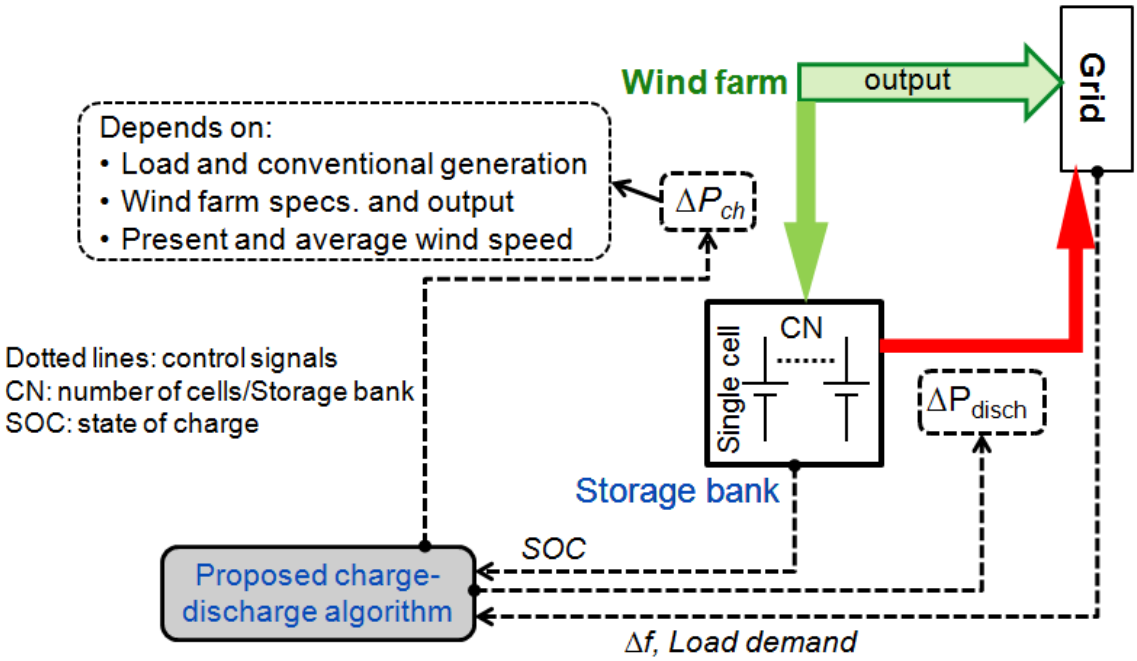

Figure 2 Major blocks and control signals of wind generation and storage bank

3.2 Support Operation

Support operation is activated when Δf violates a predetermined limit based on grid operators requirement (*in this paper Δf safe margin is -0.05 Hz* [19]) as long as SOC > SOC_{min}. Throughout Support mode, *all WFs' outputs* are exploited to cover load demand *i* even if CGC_r predetermined value is violated. The provided power step is considered to be constant (ΔP_{disch}) to curtail generation-demand mismatch. $\Delta P_{disch\text{-}i}$ is obtained using Eq(7).

$$\Delta P_{disch\ i} = Vc_i \cdot Ic_i \cdot CN_i \approx \Delta PC_{total} \cdot SCF_i \qquad \text{Eq(7)}$$

Most of the highlighted support techniques based on WTs' stored kinetic energies face the risk of causing a second frequency deviation after the depletion of extracted kinetic energy. On the contrary, SBs have fixed predetermined participation for certain defined duration (i.e. $\Delta P_{disch\ i}$ continues for certain time (TS_i) to reduce the occurrence probability of a second frequency excursion). TS starts counting when Δf reaches its safety margin for the first time after a frequency event and it is reset when Δf violates its safety limit. However, TS completion depends on SOC value such that it is forbidden to violate SOC_{min} in order to complete TS. TS_i is adjusted on a proportional basis to CN_i using Eq(8) to dispatch the WFs' contributions. Thus, the switching of all WFs from *Support to Normal* operation is not synchronized to mitigate the risks of successive frequency events and incident fluctuations. For instance, the longest TS is provided by the SB of highest CN taking into consideration

that all the cells are typical in all SBs. $TS_{longest}$ value is predetermined by operators (i.e. it is assumed to be 90s in this paper to be relevant to the average clearance duration of moderate frequency deviations), accordingly other TS values are evaluated.

$$TS_i = \frac{CN_i}{CN_{highest.}} \cdot TS_{longest} \qquad \text{Eq(8)}$$

An illustrative flowchart for the prosed operation algorithm is displayed in Figure 3.

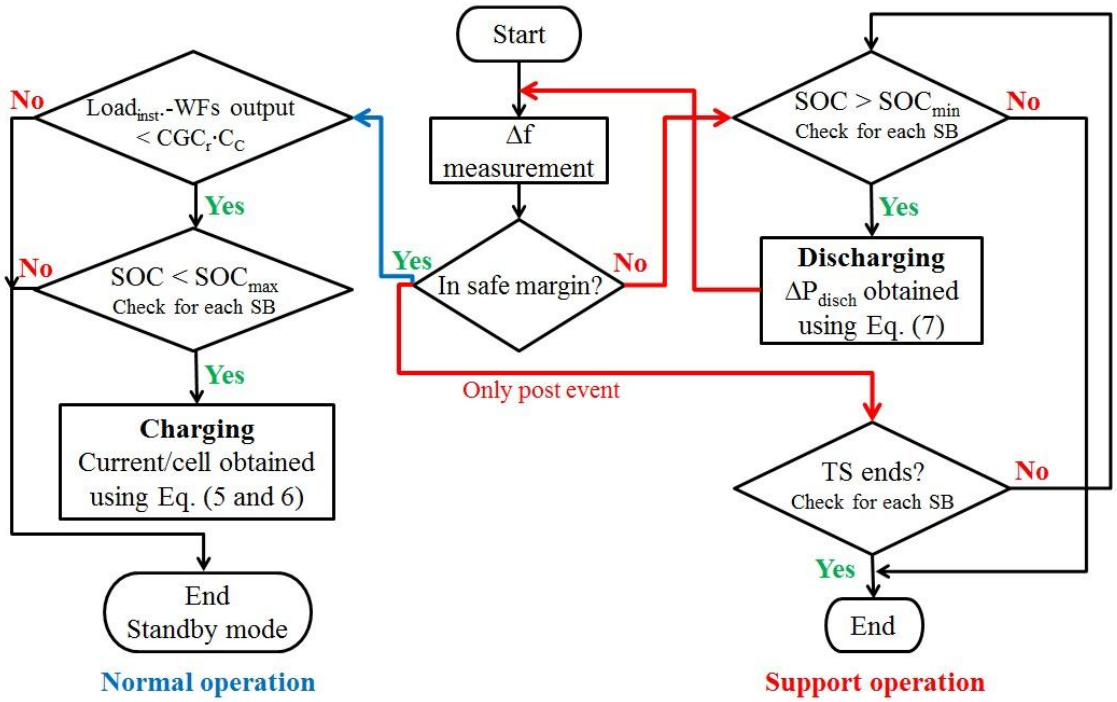

Figure 3 Operation algorithm flowchart

4. Test system

The benchmark system implemented in this research work is inspired from certain sector from the Egyptian 50 Hz grid as shown in Figure 4. The selection of Egyptian grid returns to the funding of Egyptian ministry of higher education and research to part of the presented work. It is of note that the mentioned data is related to the year 2010 (the start of the research project). Considered sector is unique due to the concentration of nine WFs candidate locations within a small geographical area so that they could be easily linked with the nearby conventional plants. C_C before wind energy integration is 3825 MW as indicated in Table (2). Generally, the accurate estimation for wind energy capacity could not be achieved due to WS intermittent nature. The actual capacity based on probabilistic and chronological estimations was in range of 25 to 45% [20]. Meanwhile, according to practical estimation in relevance to WSs records and WFs specifications in certain region, the actual capacity reached 55% [21]. In particular, this paper assumes that the integrated WFs' actual capacity is 50% from their

rated powers, markedly, 1024 MW. Thus, new C_C is 2801MW and the average wind power penetration is 27% from the former C_C.

Nine WFs, whose locations and WS_{avg} are described in Table (2) [22], replace certain portion from the former conventional capacity. Two types of WTs are integrated, namely, GE-1.5 MW and G-2 MW such that each WF includes 65 units from each type. For simplicity, and since there is no special control algorithms are integrated to the WT (i.e. all WTs follow their MPT curves), the production of both types of WTs is anticipated based one the incident WS and MPT look-up table of each type which are published by the manufacturers [23, 24].

The available WS data in each location are average WSs records every ten minutes [25]. The methodology presented in [26] is applied to get higher resolution WSs arrays, namely, 15 s time step so that the impact of WS dynamics is acknowledged.

The Egyptian grid chronological hourly load is integrated after it is de-rated by 79.9% (i.e. ratio between the concerned sector generation capacity to the whole grid capacity is 20.1%). Selected block diagrams for the integrated simulation models are present in the Appendix. Further information is found in the related references.

Figure 4 Involved Egyptian grid sector and WFs' locations

Table 2 Integrated conventional Plants and WFs

No.	WF location	$WS_{avg.}$
1	Abu Dara	8.2 m/s
2	Nabq	6.8 m/s
3	NW	10 m/s
4	ZayT NW	10 m/s
5	Ras Ghareb	9.8 m/s
6	Port Said	4.7 m/s
7	Ras Sedr	7.1 m/s
8	St. Paul	8.5 m/s
9	Nuweiba	5.5 m/s

Plant Location	Type	Capacity, MW
Port Said	Steam	682
Abu Sultan	Steam	600
Gulf of Suez 1 and 2	Steam	682
Ataka	Steam	900
Auon Moussa	Steam	640
Sharm Elsheikh	Gas	178
Hurghada	Gas	143

5. Case Studies

Base case study analyzes the system frequency response during two successive frequency excursions caused by sudden rise in load demand by 8% from its actual amount (i.e. 2838 MW) then it rises steeply again after 45 s by an additional 3%. System frequency simulation is based on the method conducted in [27]. The sudden increase in load is applied to initiate a frequency drop event. The author preferred to keep the installed generation capacity unchanged during the event; hence the frequency drop is not initiated by a sudden generation outage. In addition, the cause of frequency drop will not have an impact on the SBs support (because the support is triggered according to Δf violation which occurs in both cases), and the impact on the frequency response will be very minor.

The under-loading events are not of interest for this paper as they will cause positive frequency deviations and this is already handled in the grids by the reduction of WFs output through certain ramps defined by grid codes. In addition, the charging of SBs in the proposed algorithm is not related to frequency (except if the system is suffering a drop, charging halts), and this to avoid the intensive switching between charging/no charging due to rapid frequency fluctuations (to maintain the battery lifetime).

First and second case studies examine frequency responses after WFs integration without and with SBs installation respectively. Benchmark system single line diagram is displayed in Figure 5. It should be highlighted that the WTs operation in both cases is following the traditional MPT, and the harvested wind energy is fed to load (and charge the SB) or rejected according to the algorithm explained previously.

Figure 6 describes ΔPC_{total} variation depending on CGC_r value selection in the proposed algorithm. ΔPC_{total} is escalating almost linearly with the increase of CGC_r. As an illustration, the rising of CGC_r expands wind power rejection possibility, thus more power is available to charge the SBs. Noticeable divergence between the four sample days returns to different WSs conditions in all WFs and the chronological load demand. The spring day results are excluded from calculating ΔPC_{total} average value due to the odd and very low expected rejected power in that specific day which might be misleading to the whole performance during Spring. However, ΔPC_{total} average value for the other three days at CGC_r =70% is implied in this paper (i.e. ΔPC_{total} = 178 MW equivalent to 4.7% from the sector generation capacity, and 8.7% from the installed wind power capacity).

In this research work, only one type of storage cells is exploited for all SBs, namely, Trojan (L16RE-B) battery cell, whose characteristics are displayed in Table (3) [28]. The DOD is

assumed to be 55%; hence battery type lifetime should be obviously extended according to fabricator recommendations. Consequently, SOC_{max} = 85% and SOC_{min} = 30% while the initial SOC in all case studies is assumed to be 70%. The universal battery model, embedded in Simulink and inspired from [29], is implemented to simulate accurate SB cells responses including the storage units' losses.

SB sizing algorithm is applied on the four sample days, providing four various values for ΔPC_{total}, SCF^{2nd} at each day hence, an average value is calculated for each factor as shown in Table (4). However, the error between SCF^{1st} and SCF^{2nd} is considerable and it basically depends on the selected time span to perform the proposed sizing algorithm. The hangars areas are calculated using Eq(9), and included in Table (4).

For instance, it is assumed that all the hangars have the same height, namely, 10 m, thereupon 12 cells could be aligned vertically allowing an overall tolerance between cells of 30%. Meanwhile, the extra spacing in the horizontal distribution of cells columns and human corridors is 160% from the exact area of the horizontally spreading cells. The outcome hangar areas seem to be reasonable, especially, if compared to either substations areas or the huge WFs terrains.

$$Hangar\ area_i = \frac{CN_i}{12} \cdot cell\ base\ area \cdot 2.6 \qquad \text{Eq(9)}$$

The winter day data is selected to execute mentioned case studies since it recorded the highest superfluous of wind power. Thus, the proposed algorithm is examined at high wind energy penetration level. The simulation time for each case is one hour, namely, from 6 to 7pm since the load is relatively high and the wind power is moderate within this duration. Control signals concerning load variations and Δf which are fed to conventional plants' governors are delayed by 20 s after the first frequency event starts. This delay emphasizes the WFs and SBs impact on frequency excursion development in its early stage.

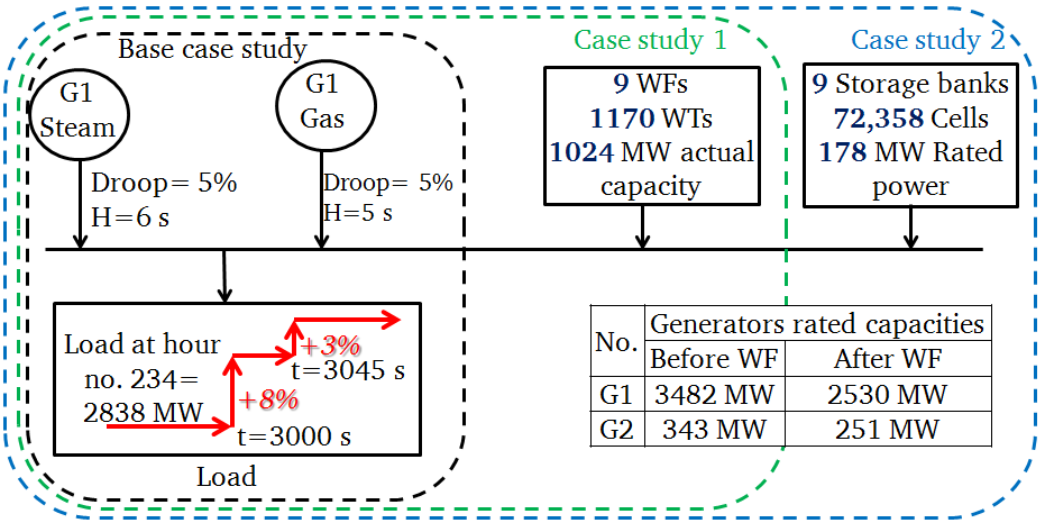

Figure 5 Benchmark system single line diagram

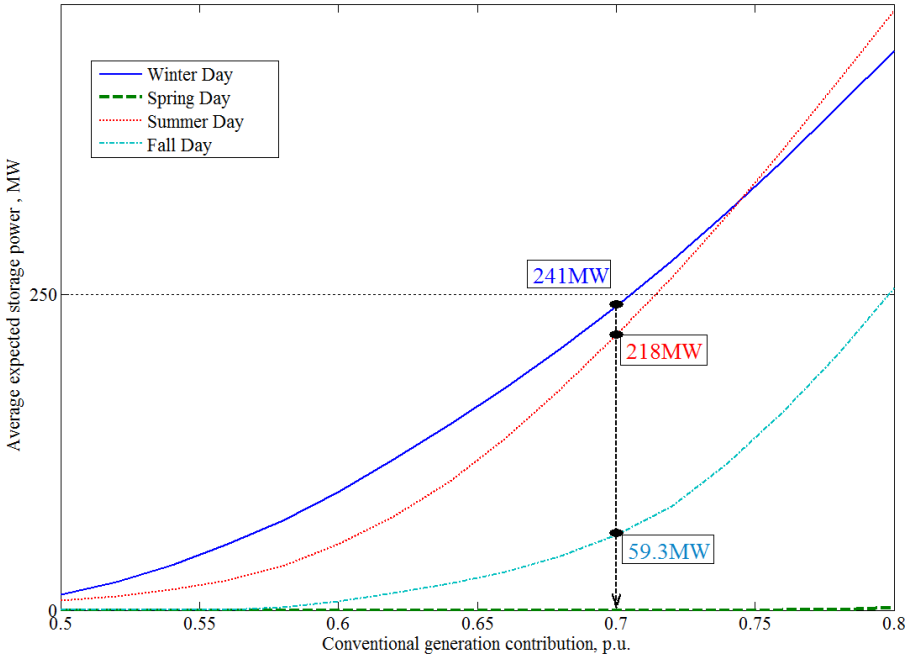

Figure 6 ΔPCtotal vs. CGCr at the four indicated sample days

Table 3 Integrated (L16RE-B) battery cell technical aspects

Rated power	C	Rated voltage	Rated current	Base area	Height
2.46 kW	410 A.H	6V	410A	1763 cm^2	61 cm

Table 4 WFs storage banks basic parameters

WF location	SCF^{1st}	SCF^{2nd}	Average SCF	TS, s	CN	Hangar area, m^2	ΔP_{disch}, MW
Ras Ghareb	0.23	0.13	0.238	90	11531	441	42.31
NW	0.19	0.13	0.185	71	8969	343	32.91
Nweiba	0.28	0.09	0.101	39	4896	187	17.97
Zayt	0.28	0.14	0.209	80	10152	388	37.25
Abu Dara	0.28	0.20	0.178	68	8658	331	31.77
Nabq	0.13	0.01	0.161	61	7805	298	28.64
Port Said	0.20	0.15	0.071	27	3439	131	12.62
St. Paul	0.24	0.11	0.173	66	8413	321	30.87
Ras Sedr	0.15	0.05	0.175	67	8494	325	31.17

This paper does not tackle the extreme case when the SOC is minimum and the system is facing a frequency event. Actually, this is very rare to happen because it means that the WS conditions were very poor in all the WFs for a long time, and the system has already faced several frequency events during this time so that all the stored energy is depleted. However, in this worst case scenario, the WTs might be equipped with certain support algorithm to provide a slight active power surge, but this is out of the focus of this paper. It is of note that this paper proposes a solution to make the WF have a defined amount of primary reserve of a very low uncertainty compared to the support algorithms which are WTG-based.

6. Results and discussion

The base case study is considered to be a reference to judge the impact of wind energy integration with and without SBs. In Figure 7, system frequency responses are displayed till 80 s after the first frequency event occurred. Practically, the frequency is oscillating all the time within an accepted margin. The WFs output variations (based on the integrated WS arrays) causes a continuous unbalance between generation and demand, hence the system frequency is always oscillating in addition to the impact of the dynamic load model. Actually, the frequency deviation will not reach zero in the integrated model because the WS is changing every 15s, thus the generation-demand balance is interrupted most of the time. However, the WS variations, leading to WFs output variations are not high enough to make the frequency deviations violate the safe margin (50 mHz). In addition, this model doesn't provide secondary frequency response (i.e. AGC), thus the frequency will not reach exactly its nominal value. However, the focus is drawn on the role of SB to provide primary response during frequency dips, to compensate the high penetration level of wind power.

The forced delay in control signals of conventional plants' governors is clear, such that the frequency started its recovery after 20s in base case. However, the integration of WFs accelerated the recovery process but it failed to reduce the maximum Δf. As shown in Figure 8, the relatively high or moderate WS in some WFs during frequency excursions caused this positive consequence. Meanwhile, the positive impact of SBs is clear since it mitigated the maximum Δf by 0.2 Hz and derived Δf to its safety margin within 6 s compared to 22 s in Case 1. Moreover, the resultant frequency fluctuations are not severe and could be handled.

In the second successive frequency event, the conventional generation reaction is not delayed; hence, the recovery process starts earlier. Nevertheless, still the positive effect of SBs is apparent such that the maximum Δf is mitigated and it reaches its acceptable threshold faster compared to Case 1. Meanwhile, the major drawback is represented by a relatively

positive Δf overshoot. In particular, the positive Δf occurring after each frequency excursion clearance is an expected result to the extra power fed by SBs within different TS duration. In other words, the SBs injected powers continue even after Δf reaches its acceptable value until TS ends. As illustrated before, the independence of SB supporting power continuity on Δf caused this overshoot. To fix this problem, $TS_{longest}$ could be shortened or ΔP_{disch} is adjusted dependently on Δf instantaneous value through certain droop function. The overshoot could also be reduced by integrating a supplement controller to the discharging process of SBs during frequency events. The controller will manage the discharging current according to the frequency deviation and/or the rate of change of frequency (RoCoF). In such way, the SBs will not just be switched between No discharging/Rated power discharging, but the discharging will vary smoothly according to the frequency event development. This could be an interesting topic for further research. However, linking ΔP_{disch} to Δf might generate high undeserved fluctuations in SBs output power leading to mitigated lifetime.

Comparing the improvements achieved in frequency responses with corresponding results in some literatures (e.g. [7, 8]) reinforces the feasibility of presented SBs support algorithm. Furthermore, these comparisons confirm that SBs transcend over several WTs support algorithms, especially from the point of view of wasted wind energy curtailment in case of SBs utilization since WTs' complicated de-loading techniques are avoided.

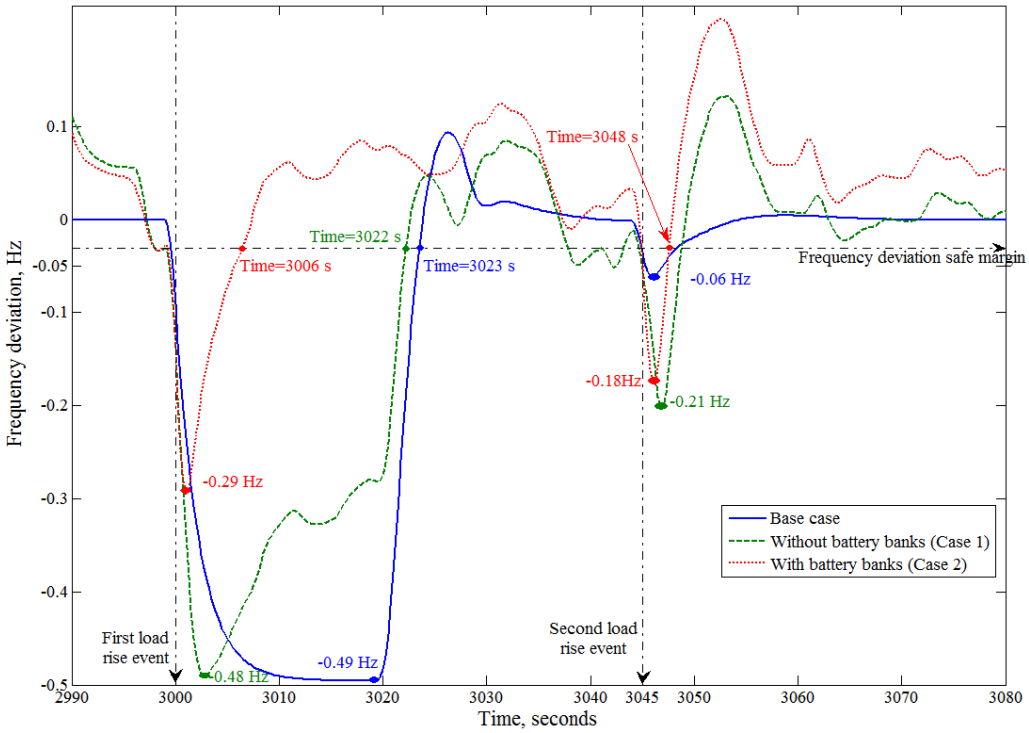

Figure 7 System frequency responses in all case studies during frequency events

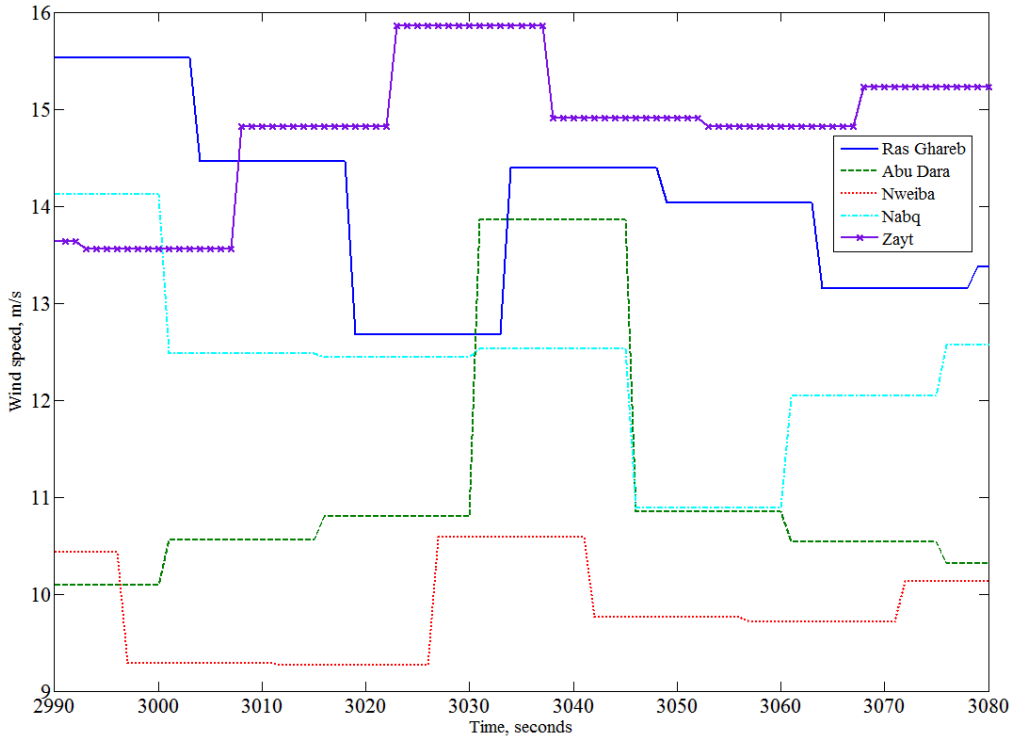

Figure 8 Wind speeds in five WFs during the frequency events

The generation variations during frequency drop clearance are considered in Figure 9. The wind power penetration in generation mix at the instant of frequency is 48%. In spite of this high WFs participation, the frequency attitude is not negatively affected, but it has slightly improved. The conventional generation is obviously reduced in Case 2 compared to Case 1 due to SBs contribution. Additionally, there is almost no deviation between steam generation curves in Cases 1 and 2. Conversely, when SBs are connected, conventional generation supplies more power to compensate the power injected by WFs to charge their connected SBs. As shown in Figure 10(a), all SBs reached SOC_{max} prior to the displayed time interval within the simulated hour (i.e. Consider that the initial SOC is 70% as mentioned earlier). The moderate WSs conditions during the considered simulation interval make the SBs get charged before the first frequency event is initiated.

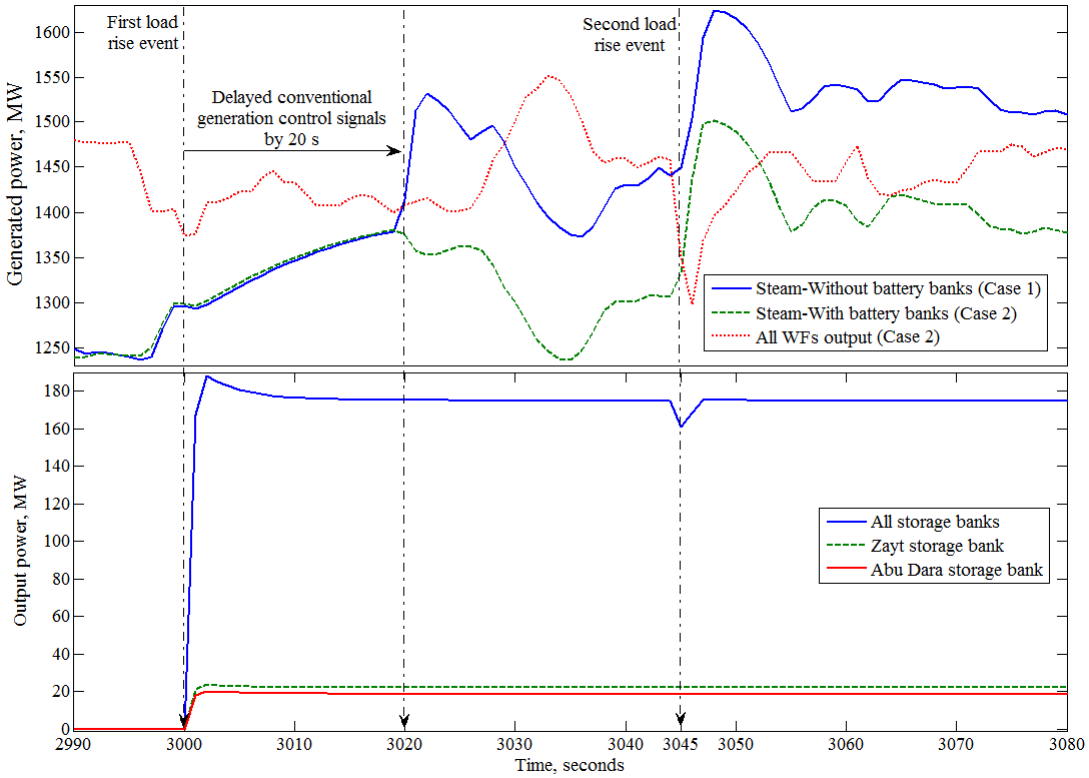

Figure 9 Conventional, WFs and storage banks output powers

The outputs of selected SBs during frequency events are shown in Figure 9. Within the first few seconds the overall output power of all SBs increases rapidly to a value (182 MW) higher than the rated power of all SBs. This returns to the voltage transient response of installed cells which implies voltage overshoots accompanied with rated currents causing this high output. After few seconds, it settles down to its normal rated power of 178 MW. It faces an intended decrease after 43 s because the TS of some SBs have run out, namely, Port Said and Nweiba SBs as indicated in Table (4). As soon as the second frequency event hits, these two SBs are switched again to Support mode and the TS is reset. It should be highlighted that the major merit of SBs over other support techniques is accentuated under these severe circumstances. As an illustration, in traditional support techniques, WTs require some time to re-store kinetic energies and attain their normal rotational speeds; hence their chances to provide further support in case of a second consecutive frequency event diminish. Conversely, the SBs can interact positively to a second frequency deviation as long as SOC is efficient whereas their reacting speed counts on the time constants of integrated batteries and installed power electronics devices. In addition, offered SBs support algorithm does not require any WS instantaneous measurements in comparison to many support techniques which count on special control algorithms. Thus, it evades from the debate of possible errors in such measurements and its possible negative influence on WTs support techniques feasibility and consistency.

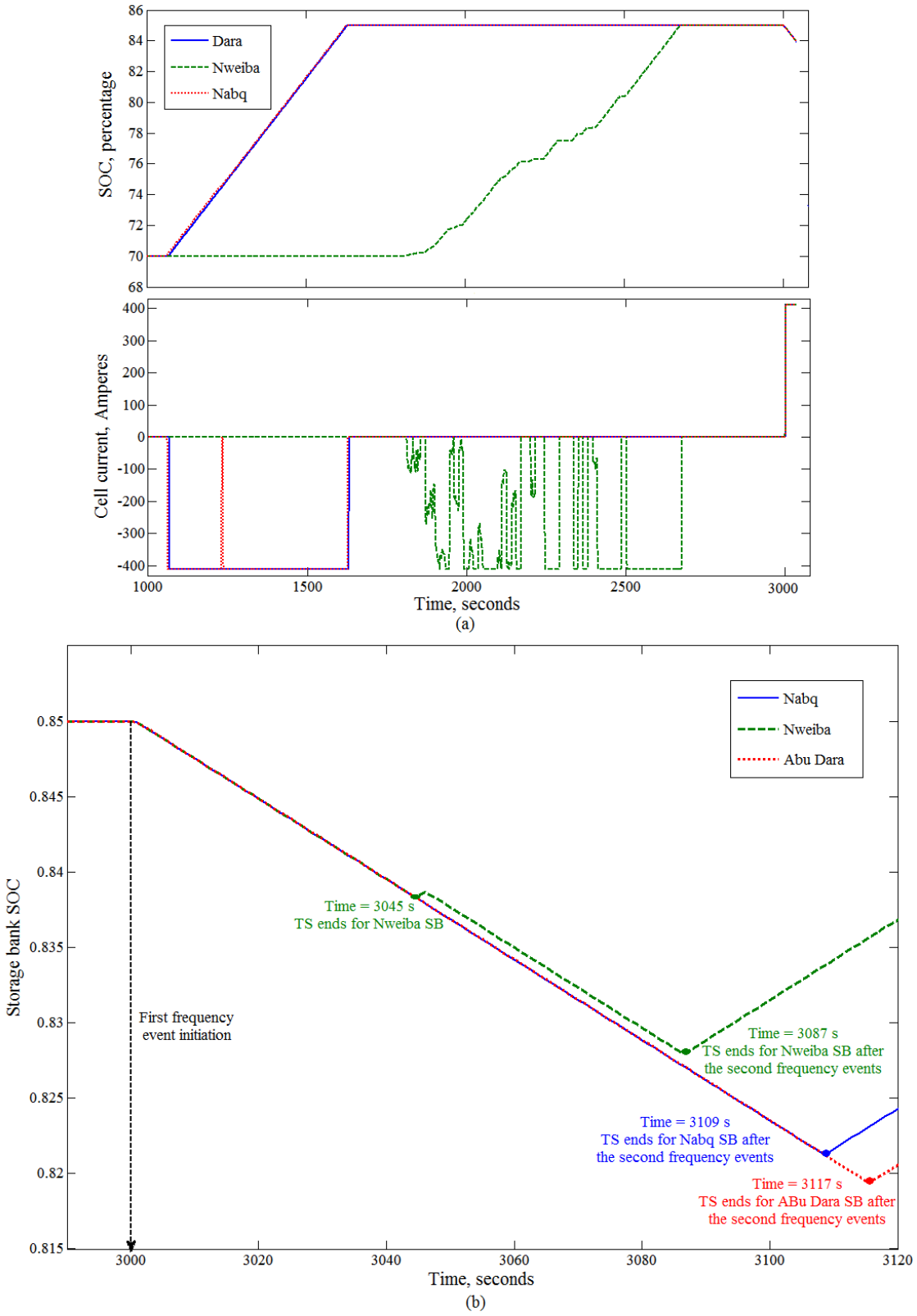

Figure 10 Selected batteries' cells internal parameters performance

The internal performances of some selected cells are also concerned in this discussion as depicted in Figure 10(b). In the proposed algorithm, the available extra wind power (i.e. utilized for SBs charging) is equally distributed among the installed cells. Therefore, the

SOCs of all cells in the same SB are typical as shown in Figure 10(b). Nweiba SOC reached its optimum value delayed compared to the other two SBs due to the poor WSs conditions, hence the WF output is barely sufficient to cover its forecasted share in load coverage and the charging power is restricted. At the excursion, all cells are discharging by the same rate because ΔP_{disch} is typical for all SBs. The same concept is insured by the charging/discharging currents attitudes of the three different cells. In particular, the discharging current is always fixed at its rated value to provide the pre-adjusted ΔP_{disch} from the whole SB. On the other hand, negative charging current is fluctuating according to WS variations which determine how much excess power is available to charge the cell (e.g. Nweiba SB). However, high WSs in Abu Dara and Nabq sites caused a fixed rated charging current which is an advantage to the cell life span. Either during charging or discharging the current is limited to its rated value to avoid any damage for the cells.

The steep changes in current variations are interpreted by the ignorance of power electronic devices delays and their transitioning stages since they are short compared to the time required by system inertial responses and frequency variations.

Figure 10(b) assures that different discharging periods are related to the pre-defined TS. The Nweiba SB has the shortest TS (39 s) with respect to Abu Dara and Nabq SB. Regarding the time instant at which Δf reaches its safe margin after the first excursion, namely, at 3006 s, the TS_{Nweiba} ends at 3045 s. Meanwhile, Abu Dara has longer TS (69 s), hence it does not end after the first frequency event, since the second excursion occurs prior to TS completion. However, it ends after Δf stabilizes in the safe region (at 3048 s as shown in Figure 7). Thus, Abu Dara discharging mode stops at time = 3048 + 69 = 3117 s as shown in Figure 10(b).

7. Conclusions

The presented research work deals with the impact of wind farms integration in power systems on frequency response at frequency drops. Battery storage banks are utilized to overcome possible drawbacks for high levels of wind power penetration in conventional grids. This paper focused on providing a feasible and detailed algorithm to estimate the power rating and energy capacity of required storage banks. Moreover, it offered a consistent algorithm to drive the installed storage bank in each wind farm either during normal operation conditions or during frequency drops. Both algorithms are implemented on certain sector in the Egyptian grid using real wind speed data. Detailed analysis for frequency responses, generation variations and cells' internal parameters fluctuations is conducted. Obtained results are motivating and designate the positive influence of applied support

algorithm on mitigating frequency excursions and the curtailment of required time to reach frequency deviation safe margin.

The superiority of SBs over other direct support techniques (e.g. de-loading) lies in: 1- avoiding of complicated controllers to apply de-loading or any other method, 2- avoiding wasting power due to direct support algorithms which most probably lead to the violation of MPT, 3- securing a predetermined amount of active power support (i.e. based on SB rating and droop), not depending on the prevailing WS conditions, 4- WS measurements are not required, 5- easier to dispatch, compared to the dispatching of WTGs inside the WF and WFs' dispatching.

In future work, improvements are planned including more complicated methods to control discharging (i.e. support power) provided by each storage bank, mainly to mitigate the possible post drop frequency deviation overshoot. Additionally, the longest continuous storage support time should be better tuned through comprehensive experiments and consistent with the frequency excursions history of the integrated grid sector. This algorithm might be also merged with traditional methods which employ storage banks as economical solutions to save wind energy during cheap tariff intervals.

8. Appendix

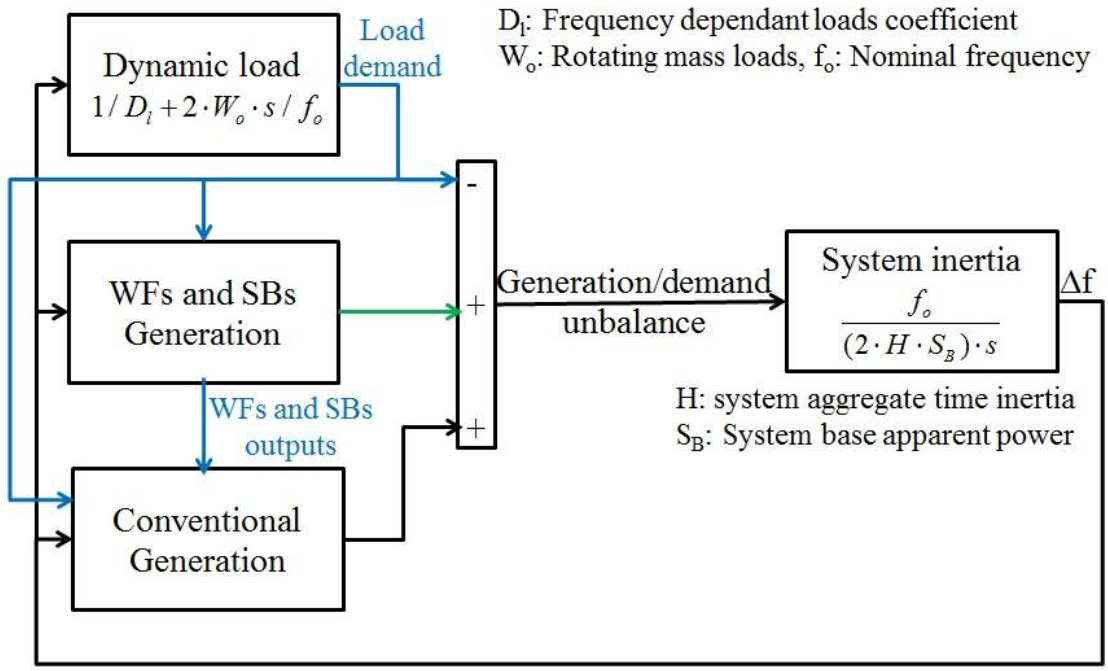

Figure A.1 Power system model

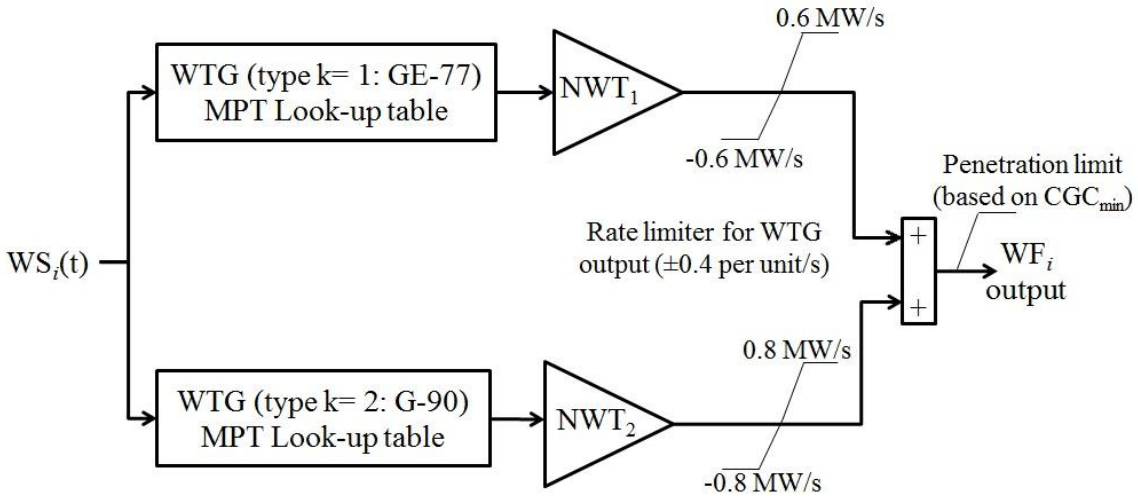

Figure A.2 Wind farm aggregate model

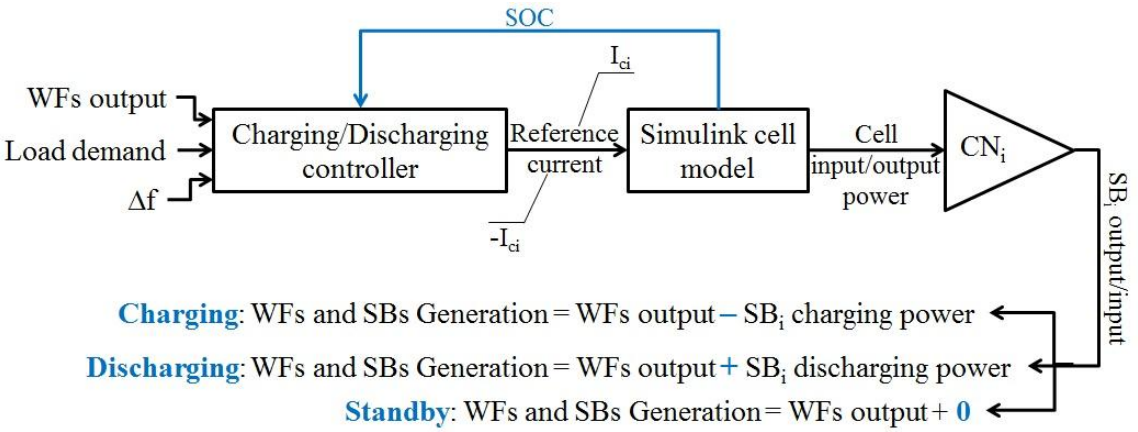

Figure A.3 Storage bank model

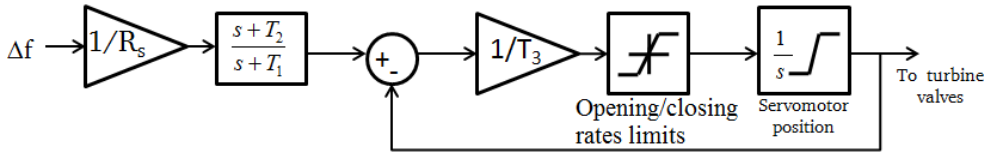

Figure A.4 Steam Turbine integrated governor

Table A.1 Integrated WTs types basic specifications

WT type	GE 77	G 90
Manufacturer	General Electric	Gameza
Rotor diameter, m	77	90
Rated WS, m/s	13	16
Rated output, MW	1,5	2
rotational speed range, rad./s	1.15 -2.51	0.94 -1.99

Table A.2 Steam Turbine and governor data[30]

Parameter	Value
T_3, seconds	0.35
Max opening and closing rates, p.u./s	0.2, -0.1
Droop (R_S)	3%
T_{CH}, T_{R1}, T_{R2} and T_{CO}, seconds	0.25, 7.5, 7.5 and 0.4

Hint: Implemented gas power plant model is available in [31].

9. References

1. Ye, W., et al., *Methods for Assessing Available Wind Primary Power Reserve.* Sustainable Energy, IEEE Transactions on, 2015. **6**(1): p. 272-280.
2. Holttinen, H., et al., *Currents of Change.* IEEE Power & Energy Magazine, 2011. **9**(6): p. 47-59.
3. B. Fox, et al., *Wind Power Integration*. IET Power and Energy Series. 2007: IET.
4. Z. Meng, *An improved equivalent wind method for the aggregation of DFIG wind turbines*, in *IEEE International Conference on Power System Technology (POWERCON)*. 2010: China.
5. B. G. Rawn, M. Gibescu, and W. L. Kling, *Kinetic Energy from Distributed Wind Farms: Technical Potential and Implications*, in *IEEE Innovative Smart Grid Technologies Conference Europe*. 2010: Sweden.
6. Attya, A.B.T. and T. Hartkopf, *Control and quantification of kinetic energy released by wind farms during power system frequency drops.* Iet Renewable Power Generation, 2013. **7**(3): p. 210-224.
7. Ruttledge, L., et al., *Frequency Response of Power Systems With Variable Speed Wind Turbines.* IEEE Transactions on Sustainable Energy, 2012. **3**(4): p. 683-691.
8. Margaris, I.D., et al., *Frequency Control in Autonomous Power Systems With High Wind Power Penetration.* IEEE Transactions on Sustainable Energy, 2012. **3**(2): p. CP2-199.
9. Chang-Chien, L.-R. and Y.-C. Yin, *Strategies for Operating Wind Power in a Similar Manner of Conventional Power Plant.* IEEE Transactions on Energy Conversion, 2009. **24**(4): p. 926-934.
10. Attya, A.B. and T. Hartkopf, *Penetration impact of wind farms equipped with frequency variations ride through algorithm on power system frequency response.* International Journal of Electrical Power & Energy Systems, 2012. **40**(1): p. 94-103.
11. Juan A. Martinez, *Modeling and Characterization of Energy Storage Devices*, in *IEEE Power and Energy Society General Meeting*. 2011: Detroit Michigan.
12. Attya, A.B. and T. Hartkopf, *Utilizing stored wind energy by hydro-pumped storage to provide frequency support at high levels of wind energy penetration.* Iet Generation Transmission & Distribution, 2015. **Accepted**.
13. Brekken, T.K.A., et al., *Optimal Energy Storage Sizing and Control for Wind Power Applications.* IEEE Transactions on Sustainable Energy, 2011. **2**(1): p. 69-77.
14. Hartmann, B. and A. Dan, *Cooperation of a Grid-Connected Wind Farm and an Energy Storage Unit-Demonstration of a Simulation Tool.* Ieee Transactions on Sustainable Energy, 2012. **3**(1): p. 49-56.
15. Teleke, S., et al., *Control Strategies for Battery Energy Storage for Wind Farm Dispatching.* Ieee Transactions on Energy Conversion, 2009. **24**(3): p. 725-732.
16. Teleke, S., et al., *Rule-Based Control of Battery Energy Storage for Dispatching Intermittent Renewable Sources.* Ieee Transactions on Sustainable Energy, 2010. **1**(3): p. 117-124.
17. Yao, D.L., et al., *A Statistical Approach to the Design of a Dispatchable Wind Power-Battery Energy Storage System.* Ieee Transactions on Energy Conversion, 2009. **24**(4): p. 916-925.
18. Li, Q., et al., *On the Determination of Battery Energy Storage Capacity and Short-Term Power Dispatch of a Wind Farm.* IEEE Transactions on Sustainable Energy, 2011. **2**(2): p. 148-158.
19. UCTE, *Appendix 1 — Load-Frequency Control and Performance*. 2002, The Union of the coordination of the transmission of electricity.
20. Castro, R.M.G. and L. Ferreira, *A comparison between chronological and probabilistic methods to estimate wind power capacity credit.* Ieee Transactions on Power Systems, 2001. **16**(4): p. 904-909.
21. Gevorgian, V., Y. Zhang, and E. Ela, *Investigating the Impacts of Wind Generation Participation in Interconnection Frequency Response.* IEEE Transactions on Sustainable Energy, 2014. **PP**(99): p. 1-9.
22. *The annual report*. 2010, Egyptian ministry of Electricity and Energy: Cairo.
23. *Brochure of Wind Turbine: G-90-2.0 MW*. 2011, Gameza Company: Spain.
24. Miller, N.W., et al., *Dynamic modeling of GE 1.5 and 3.6 MW wind turbine-generators for stability simulations.* 2003 Ieee Power Engineering Society General Meeting, Vols 1-4, Conference Proceedings, 2003: p. 1977-1983.
25. N. G. Mortensen and U.S. Said, *Wind Atlas for Egypt*. 2009, New and Renewable Energy Authority: Cairo.
26. Attya, A.B. and T. Hartkopf. *Generation of high resolution wind speeds and wind speed arrays inside a wind farm based on real site data*. in *Electrical Power Quality and Utilisation (EPQU), 2011 11th International Conference on*. 2011.
27. Kundur, P., *Power System Stability and Control*. 1994, New York: McGraw-Hill Inc.
28. *Energy Storage Solutions for Renewable Energy series manual*. 2012, Trojan Battery Company: USA.
29. Ceraolo, M., *New dynamical models of lead-acid batteries.* IEEE Transactions on Power Systems, 2000. **15**(4): p. 1184-1190.

30. *DYNAMIC MODELS FOR STEAM AND HYDRO TURBINES IN POWER-SYSTEM STUDIES.* Ieee Transactions on Power Apparatus and Systems, 1973. **PA92**(6): p. 1904-1915.
31. H. Emam Shalan, M. A. Moustafa Hassan, and A. B. G. Bahgat, *Parameter Estimation and Dynamic Simulation Of Gas Turbine Model In Combined Cycle Power Plants Based On Actual Operational Data.* Journal of American Science, 2011. **7**(5): p. 303-310.